

www.acsaem.org Article

Characterizing the Microstructure of Separators in Lithium Batteries and Their Effects on Dendritic Growth

Andrew Cannon and Emily M. Ryan*



Cite This: ACS Appl. Energy Mater. 2021, 4, 7848–7861

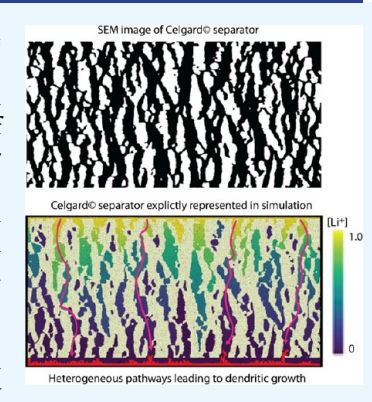


ACCESS

III Metrics & More

Article Recommendations

ABSTRACT: Porous separators are used to physically separate the electrodes in batteries while providing mechanical stability and improving the performance of lithium batteries. In this study, the effect of the battery separator microstructure on mass transport and lithium dendrite growth is investigated using pore-scale computational modeling. The microstructural characteristics of the separator, such as porosity, tortuosity, and constrictivity, directly alter diffusion paths for lithium ions during battery cycling. The accuracies of experimental relations, i.e., Bruggeman, MacMullin, used to determine these characteristics are unreliable. A pore-scale computational model is used to simulate mass transport and dendrite growth, utilizing an explicit representation of the separator microstructure. The simulation is compared to the experimental relations and shows that the experimental relations fail to adequately capture important physical characteristics in the microstructure of the separator. Tortuosity, a characteristic that is difficult to experimentally measure, is shown to significantly affect the growth rate of dendrites and can lead to a shorter lifetime in the battery. Additionally, the degree of heterogeneity in a battery



separator is explored and shown to lead to different dendrite growth rates even when the bulk physical characteristics of separators are the same. Evidence provided in this paper suggests that neglecting local variation of these properties can lead to nonuniform diffusion and, in turn, problematic dendritic growth. The findings offer insight into properties not often considered in battery separator designs.

KEYWORDS: lithium-metal batteries, battery separator, dendrite, microstructure, heterogeneity, mass transport, tortuosity

1. INTRODUCTION

Advances in alternative energy generation from photovoltaics and wind turbines to the emergence of electric vehicles have created increasing demands for advanced high-energy-density batteries. The Intergovernmental Panel on Climate Change has identified battery development as crucial to further implementing renewable energy sources and distancing ourselves from fossil fuels. One of the most promising battery technologies is lithium-metal batteries (LMBs). This technology has the potential to substantially increase both the energy and power density compared to current state-of-the-art lithium-ion batteries. ²

However, LMBs have a number of challenges, such as safety and cyclability, to overcome before they are commercially viable.³ In particular, the formation of dendrites at the electrolyte—electrode interface is one major challenge that directly affects battery performance. Dendrite formation can cause a range of issues, from decreasing the capacity of the battery to causing a short circuit and subsequent fire.^{4,5} Dendrites form after multiple charge/discharge cycles and are primarily caused by a nonuniform plating of lithium (Li) metal. Uneven plating can be attributed to a combination of defects on the anode surface and nonuniform current density or mass transport.⁶ Defects on the surface, such as pits, cracks, grain

boundaries, or impurities, can serve as nucleation sites for dendrites. By simply roll pressing the anode surface, Becking et al. have demonstrated that mechanically flattening much of the surface roughness can significantly increase the cyclability of lithium-metal batteries when compared to the use of native lithium-metal anodes. Additionally, when the ionic current reaches a critical density in a certain location, dendrite growth in that location becomes thermodynamically favorable. So nonuniform current density drives increased metal deposition during charging in some areas and more stripping during discharge in others, increasing the probability of dendritic growth. ^{9–11}

One of the main components of the battery that drives nonuniform mass transport through the electrolyte is the porous separator, which is primarily used to physically isolate electrodes and prevent short circuits. Recent investigations have begun to develop separators that have additional functionalities in the

Received: April 27, 2021 Accepted: July 14, 2021 Published: July 28, 2021





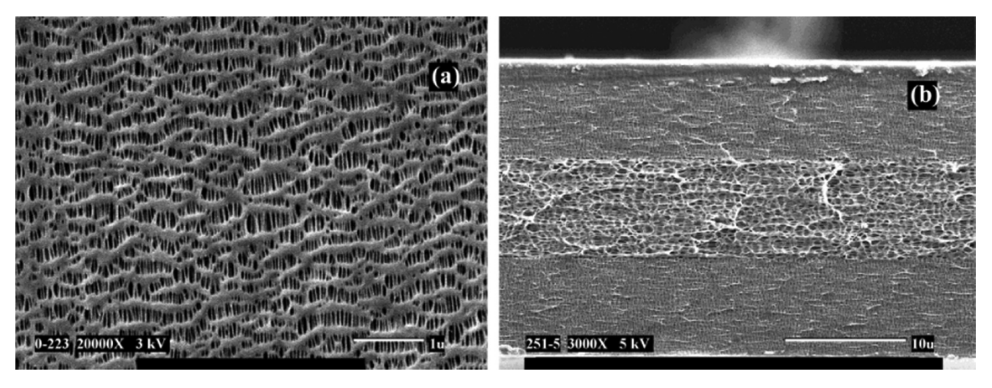


Figure 1. SEM of a Celgard 2325 separator used in lithium-ion batteries: (a) top view and (b) cross section. Reprinted with permission from.³⁷ Copyright 2004 American Chemical Society.

battery system.¹² These functionalities are, in general, of two types: improved mass transport and disruption of dendritic growth on the anode surface.

To improve mass transport, some researchers increased the wettability of separators. Increased separator wettability leads to increased Li-ion conductivity and transference number. Yang et al. 13 and Nie et al. 14 have turned to biology for inspiration; their separators are coated with a layer of biologically inspired nanofibers. These layers increase electrolyte wettability and redistribute Li ions at the molecular level which both increase the ionic diffusion and enable a more uniform ionic flux. Wang et al. 15 used a two-dimensional hexagonal VS $_2$ flake to assemble "nanotowers" on the surface of the separator. The nanotowers have "lithiophilic" properties which encourage uniform ionic deposition on the anode surface. On the other hand, Rajendran et al. recently demonstrated the potential of a carbon nanomembrane to regulate ion transport through a Celgard membrane. 16

Other investigations focus on the disruption of dendritic growth along the anode surface. Zhang et al. 17 suggest that simply maintaining consistent pressure in the battery cell can suppress dendrites. They demonstrate that at a critical pressure, dendritic growth halts, but deposition continues along the anode and does not impeding battery charging. Liang et al. 18 developed a separator coating that prevents dendrites from penetrating the separator by deflecting dendrites with a "nanoshield." These nanoshields have a larger curvature (than the separator), which redirects the tip of the dendrite away from the separator. Lee et al. 19 coated the anode side of a commercial separator with an ultrathin layer (<100 nm) of copper. The thin coating does not block the pores of the polyethylene separator but acts as a secondary current collector where Li ions can deposit (in addition to the anode). These researchers report an increase in cycling stability and a reduction in "dead" lithium, which are both attributed to the manipulation of the dendrite morphology.

While these recent advances show promise, in this work, evidence is presented that one of the main sources of the nonuniformity is the microstructure of the separator. This claim is supported by experimental researchers who have created ultrafine²⁰ and nanoporous^{21,22} membranes. These novel membranes are able to enforce a more uniform ionic flux to the anode surface by creating a homogeneous microstructure. The microstructures of the separator (geometrical parameters such as porosity, tortuosity, and constrictivity) are one of the main determinants of the mass transport through the separator. However, these parameters can be difficult to experimentally measure and define; previous research has attempted to establish

relationships and correlations between these parameters.^{23–29} Other methods for measuring these parameters involve computationally meshing the porous network and then calculating distributions of parameters.³⁰ While these methods may be useful in some fields, such as subsurface transport,³¹ they overly simplify the geometric parameters of battery separators. The small scales at which batteries operate heighten the importance of the precise measurement of these parameters.

The microstructure of the separator also affects the structural integrity of the separator. Kalnaus et al.³² tested several popular battery separator's mechanical behavior. They concluded that Celgard separators display strong anisotropy and heterogeneity, which decreases the mechanical integrity of the separator. This characteristic behavior provides further evidence that heterogeneous geometrical parameters can lead to critical strain failure in battery separators.

Furthermore, most methods for quantifying these geometrical parameters, whether via experimental measurement or correlations, are only able to determine bulk values, disregarding any heterogeneities in the structure.³³ These heterogeneities create a nonuniform current density that directly influences dendritic growth; therefore, regulating the separator's heterogeneity can lead to better control of dendrite growth^{24,34} and charging efficiency.^{6,35}

Experimental measurement and characterization of separators at a pore scale is challenging, but computational modeling is able to resolve this scale. Our previous studies have explored the effect that simple structures have on dendrite morphology.³⁶ In this study, we build on those findings and present a pore-scale computational model using explicit separator structures to explore the effects of porosity, tortuosity, and constrictivity on mass transport and dendrite growth, and how heterogeneities affect dendrite growth. This paper discusses the details of the computational model along with parametric studies looking at how separator geometry affects the mass transport through the electrolyte and dendrite growth rates. Finally, with advanced imaging and processing of Celgard separators by Wood et al.,33 there are now detailed structural representations of commercially available separators, in addition to their electrochemical properties. These digital representations of porous separators are explicitly reconstructed inside the model and comparisons are made to experimental measurements. The effects of nonuniformity on both simplistic and realistic structures of porous battery separators are shown, which will provide insight into future considerations for the design of battery separators.

2. BACKGROUND

Porous separators are commonly produced by first extruding a polymer (polypropylene or polyethylene) and then by stretching it to create micro tears that act as pores, Figure 1. These materials are used because they are relatively inexpensive and stable. Complex pathways through the separator are often created by the micro tears; researchers are also developing novel separators that have pathways created from different manufacturing processes.³⁸ The thickness of the separator is typically $25-40~\mu m$ for commercial Li-ion batteries.³⁹

The increased diffusion length through the pathways of the separator reduces the effective diffusivity and ionic conductivity of the electrolyte. The combined effects of the separator and electrolyte on diffusivity (or ionic conductivity) are referred to as the effective diffusivity, $D_{\rm eff}$ (effective ionic conductivity, $\sigma_{\rm eff}$), to differentiate it from the inherent molecular diffusivity (conductivity) of the electrolyte, D_0 (σ_0). The ratio of the molecular diffusivity (conductivity) to the effective diffusivity (conductivity) is known as the MacMullin number $^{41-44}$

$$N_{\rm m} = \frac{D_{\rm o}}{D_{\rm eff}} = \frac{\sigma_0}{\sigma_{\rm eff}} \tag{1}$$

The value of the effective diffusivity (conductivity) is the result of the physical characteristics of the porous separator, such as porosity, tortuosity, and pore size. Additionally, the separator thickness, permeability, and constrictivity are known to affect local mass transport and are critical to battery performance.³⁷

The porosity, ε , is the ratio of nonsolid volume to the total volume, usually ranging from 0.35 to 0.6 for battery separators.³⁹ There are many experimental techniques for determining porosity.⁴⁵

The constrictivity, β , is defined as

$$\beta = \frac{A_{\min}}{A_{\max}} \tag{2}$$

where A_{\min} is the minimum cross-sectional area along the pore and A_{\max} is the maximum cross-sectional area along the pore.

The tortuosity, τ , is a more complicated property to define and determine. The literature defines a few types of tortuosity. The most common tortuosity is defined by the ratio of the shortest length of a path (L) through the nonsolid volume to the thickness (t) of the separator 42,46

$$\tau = \frac{L}{t} \tag{3a}$$

However, this definition does not consider pore size changes along the path which are characterized by the constrictivity, β . Accounting for pore size via the constrictivity leads to the geometric tortuosity ($\tau_{\rm geo}$)⁴⁷

$$\tau_{\rm geo} = \frac{L}{\beta t} \tag{3b}$$

Directly measuring tortuosity using experimental techniques is challenging, and so correlations have been developed. These correlations were first used to analyze sediment and porous materials. One method is measuring the time it takes to pump $100~\rm cm^3$ of air through an area of $6.45~\rm cm^2$ of a porous medium under a pressure differential of $1.22~\rm kPa$. This time is known as the Gurley Number and is thought to be related to the tortuosity. 42,48

Another method was developed for diffusion along capillary paths. 44 It relates the ratio of the porosity and tortuosity as

$$N_{\rm m} = \frac{\tau}{\varepsilon} \tag{4}$$

With the porosity and MacMullin number known, the tortuosity is solved for.

The tortuosity is also calculated using a simple empirical correlation with the porosity. This correlation was initially explored in the hydrology field, 46 but adaptations have been made to make it applicable to other fields such as electrochemistry. The most common adaptation is the Bruggeman relation 49,50

$$\tau = \gamma \varepsilon^{1-\alpha} \tag{5}$$

where α , the Bruggeman exponent, typically has a value of 1.5 or 2, and γ , a geometric fitting parameter, takes a value of 1 when the porous media is made of spherical particles. These values are typically used for battery materials. Variations of the Bruggeman equation and other phenomenological relations have been reported to relate porosity and tortuosity; ⁵¹ however, this work will focus on the Bruggeman relation as it is the most common relation used for electrochemical systems. By combining eqs 4 and 5, the relationship between $N_{\rm m}$ and the physical parameters becomes

$$N_{\rm m} = \varepsilon^{-\alpha} \tag{6}$$

where γ is equal to 1. Equation 6 can be used to predict the effective diffusivity through a porous separator or the tortuosity when the diffusivity of the electrolyte is known.⁵²

Another important consideration in designing battery separators is their homogeneity. The microstructural characteristics of the separator are not uniform. Manufacturers of battery separators typically provide an average value for the porosity and thickness of separators and researchers³³ report bulk values of electrochemical properties (i.e., mass transport). These bulk parameters use a macro-homogeneous approach to characterizing the separator and ignore the heterogeneous nature of the structure. In the research reported in this paper, the local characteristics of simplified porous separators are measured and structural data of Celgard polypropylene separators are recreated from SEM images.⁵³

Ultimately, the physical characteristics of the battery separator contribute to a decrease in mass transport in the electrolyte. The magnitude and location of this decrease can change the morphology of the dendrite structure along the anode surface. At higher local effective diffusivities, the dendrite morphology is controlled by the reaction rate. ⁴ The Li deposition in this regime across the anode surface creates uniform plating or small bushlike dendrites. However, when the effective diffusivity is lowered by decreasing the porosity or increasing the tortuosity of the separator, the morphology becomes controlled by the mass transport. The structure of the dendrite is longer, thinner, and has more branches. This mass transport limited regime is where problematic dendrites occur. The thinner dendrites are more likely to break off the anode, forming "dead" lithium, and the longer dendrites can penetrate the battery separator and cause a short circuit and cell failure. 54

3. METHODS

3.1. Pore-Scale Smoothed Particle Hydrodynamics Model. Pore-scale computational modeling is used to study the reactive

Pore-scale computational modeling is used to study the reactive transport near the electrode—electrolyte interface in a Li battery to understand how local mass transport affects dendrite growth. A Lagrangian, particle-based method known as smoothed particle hydrodynamics (SPH) is used to model the reactive transport through

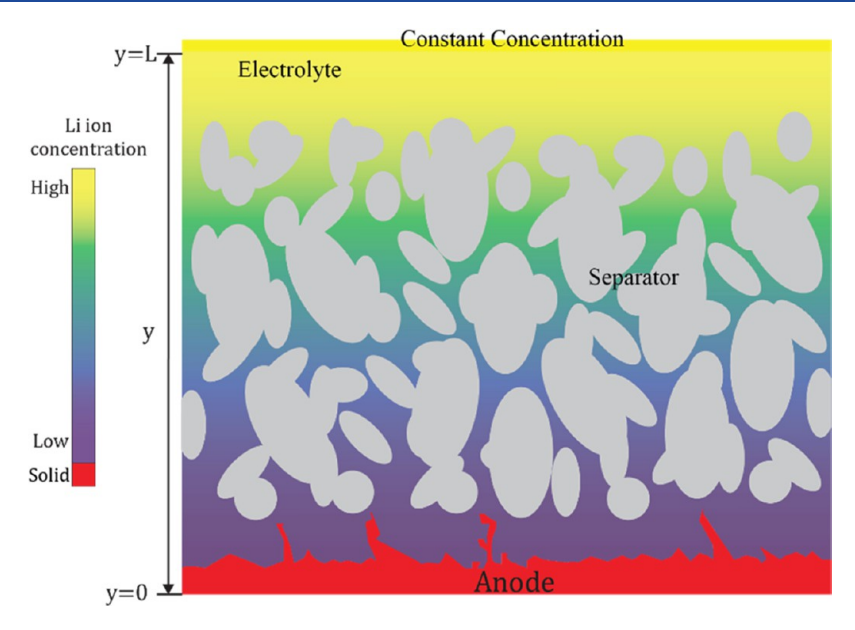


Figure 2. Schematic of the simulation domain. The anode and dendrite growth are represented in red along the bottom and the separator in the electrolyte is represented by the gray objects.

the separator and the dendrite growth at the anode surface, as shown in the schematic of Figure 2. The model explicitly resolves the separator structure and does not rely on the porous media parameters, such as correlational values or experimental fits of porosity, tortuosity, or pore size, as inputs. This allows the model to directly calculate these values and investigate their effects on dendrite growth. The gray geometries in the schematic of Figure 2 represent the battery separator, which are nonreactive solids that restrict the transport of Li⁺, and the red structure represents the anode, which is the initial reactive surface and subsequent dendritic growth.

The SPH model used for this work is based on a previously published SPH model of dendrite growth in a Li battery, which has been verified via analytical solutions and qualitatively validated by comparison to experimental imaging of dendrite growth. ^{36,55,56} To simulate reactive transport near the interface, the governing equation is the species conservation equation

$$\frac{\partial C(x, y, t)}{\partial t} = \nabla \cdot (D\nabla C(x, y, t)), \ r \in \Omega_{F}$$
 (7)

where Ω_F is the fluid domain (electrolyte solution), D is the diffusivity, and C is the Li⁺ concentration. It is assumed that the Li-ion transference number does not change significantly in the range of concentrations studied and, therefore, only diffusivity drives the concentration change in the electrolyte. ⁵⁷

A uniform initial concentration is assumed throughout the domain

$$C(x, y, t = 0) = C_0 (8)$$

and a constant concentration is applied outside the diffusion layer for the duration of the simulation ${\bf r}$

$$C(x, y = L, t) = C_1 \tag{9}$$

Equation 7 governs the diffusion of Li⁺ through the finite diffusion layer near the anode surface. Along the bottom of the simulation domain is the reactive anode surface, and a first-order reaction boundary condition is applied

$$D\nabla c_i(r_s, t) = K(c(r_s, t) - C_{eq}), r_s \in \Gamma, t > 0$$
(10)

where r_s is a point along the reactive surface Γ and \vec{n} is the unit vector normal to the reactive boundary Γ , which points outside of the fluid domain $\Omega_{\rm F}$. $C_{\rm eq}$ is the equilibrium concentration for the solidification reaction and K is the reaction rate coefficient. Dendritic growth occurs along the anode surface, which is the result of Li⁺ ions combining with

electrons in a nonuniform manner. As dendrites grow, they form the new reactive surface (Γ) that creates sites for future dendrite growth.

The simulations presented here focus on the effect the separator microstructure has on mass transport in the bulk electrolyte and the reactive mass transport at the anode-electrolyte interface. As such, a number of simplifications are made to allow isolation of the mass transfer and separator microstructure effects. These simplifications include a concentration-independent diffusivity, which is common for the range of concentrations used in this study; 10,58 neglecting the mechanical dendrite-separator interaction (the simulation is ended before critical dendrite penetration of the separator); not including potential or electro-convection effects; and ignoring secondary reactions. These types of simplifications are commonly used in modeling to isolate particular phenomena, and some of these effects are the focus of further research in our group. Further, in line with other models of interfacial physics, such as phase-field models,⁵⁹ transport and dendritic growth are considered two dimensions. While there may be some discrepancy between the results of 2-D simulations and 3-D experiments, there is still a great deal of value in understanding the essential interaction between the separator geometry and mass transport. These simplifications are made to isolate the direct effects the separator microstructure has on the reactive mass transport and dendrite growth but are not meant to be a complete model of battery physics, which is an ongoing area of research in our own laboratory and the broader computational modeling community.

The governing equation (eq 7) is discretized using the SPH method as discussed in Tan et al. 11,36 and is implemented in the LAMMPS code base. 63 The LAMMPS implementation extends a previous implementation of the energy equation 64 to include multispecies reactive transport. 65 The implementation has been verified in Tan et al. $^{65-67}$

3.2. Effective Diffusivity Calculations. To calculate effective diffusivity through the separator, first a 2-D simulation is conducted with the desired microstructure and electrolyte with a diffusivity, D_0 . This microstructure restricts the diffusion of the Li $^+$ through the liquid electrolyte. The 2-D simulation is collapsed into a 1-D average concentration profile. The concentration profile is then used as the solution to the 1-D diffusion equation

$$\frac{\partial^2 C}{\partial^2 x} = D \frac{\partial C}{\partial t} \tag{11}$$

with constant concentration at the boundaries, C_1 at x = 0 and C_2 at x = l, and an initial concentration of C_0 across the entire domain, 0 < x < l. The solution for these conditions is laid out by Crank⁶⁸

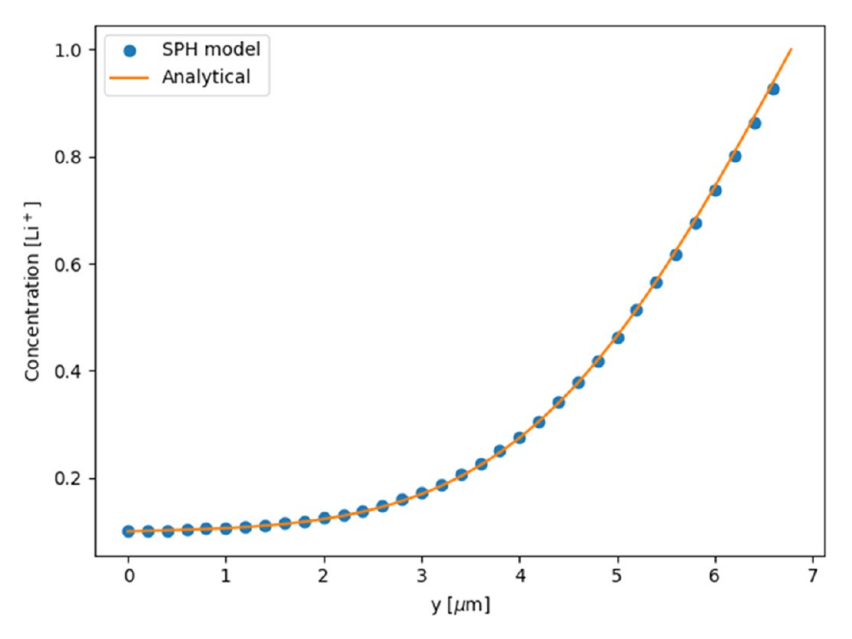


Figure 3. Local electrolyte concentration vs. position in the electrolyte for both the analytical solution (eq 12) and the SPH model.

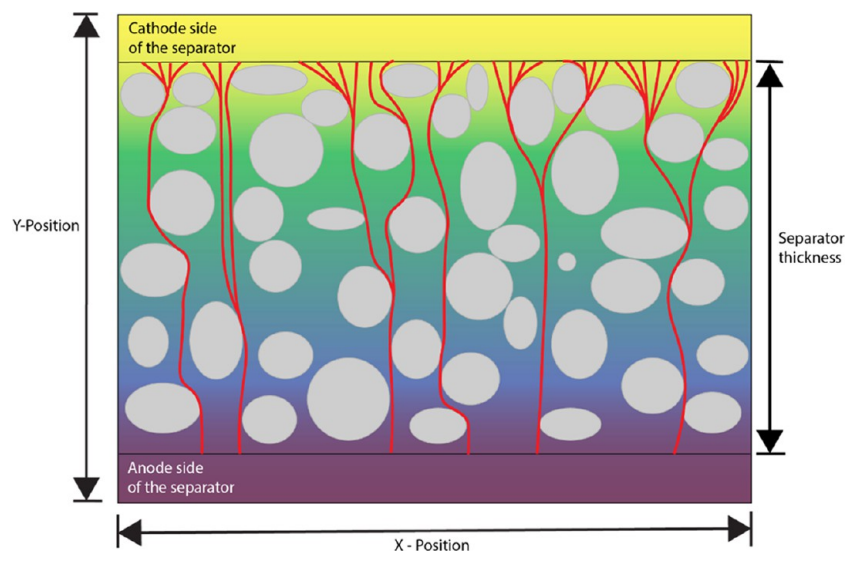


Figure 4. Diagram of the tortuosity paths (red lines) calculated using the shortest path methods.

$$C(x, t) = C_1(C_2 - C_1)\frac{x}{l} + \frac{2}{\pi} \sum_{n=1}^{\infty} \frac{C_2 \cos n\pi - C_1}{n} \sin \frac{n\pi x}{l}$$

$$\exp(-Dn^2\pi^2t/l^2) + \frac{4C_0}{\pi} \sum_{m=0}^{\infty} \frac{1}{2m+1}$$

$$\sin \frac{(2m+1)\pi x}{l} \exp\{-D(2m+1)^2\pi^2t/l^2\}$$
(12)

The concentration profile, C(x,t), from the simulation is the solution to eq 12, and the diffusivity, D, is calculated. This calculated diffusivity implicitly includes information about the diffusion through the separator and therefore is now the effective diffusivity, $D_{\rm eff}$.

This method is verified by calculating the diffusivity predicted by the SPH model for 1-D diffusion in a single phase. As shown in Figure 3, the model accurately predicts the diffusion when compared to the analytical solution, and the diffusivity calculated by the predicted concentrations $(9.514 \ \mu \text{m}^2/\text{s})$ is within 5% of the actual diffusivity $(10 \ \mu \text{m}^2/\text{s})$. This small discrepancy can be attributed to the disordered particle distribution, which creates some noise in the model.

3.3. Calculating Tortuosity. In this study, the exact definition of tortuosity given in eq 3b is considered. With computational methods, the tortuosity can be calculated using path planning methods from computer science. In our pore-scale SPH model, the porous structure is explicitly modeled and therefore the exact structural information about the separator is known. Using the A*69 and Dijkstra's shortest path algorithms, 70,71 widely used in the computer science field for path planning, the guaranteed shortest distance between two points is found, or in this case, between a point and a side. Figure 4 illustrates the tortuosity paths calculated using these methods. Starting at each computational point (particle) along the cathode side of the separator, the path (red lines) to reach the other side near the anode is determined. The path length divided by the separator thickness gives the tortuosity at each starting location. These path lengths can then either be averaged along the surface of the entire separator to give a bulk tortuosity value or divided into bins along the surface to give a local tortuosity value.

3.4. Breakthrough Time. The effects of geometric parameters on dendrite growth are quantified using a breakthrough time. This time is defined as the time it takes dendrite growth to reach the bottom of the separator, which we set as our breakthrough line (Figure 5). This metric

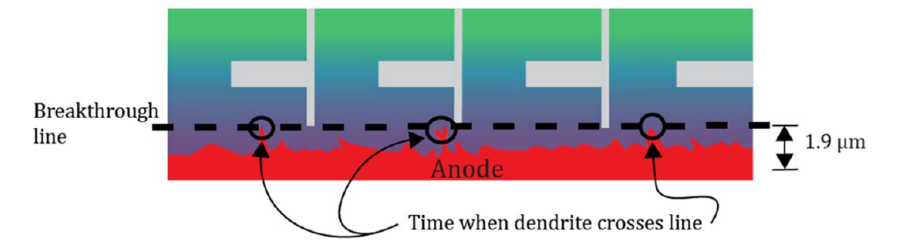


Figure 5. Diagram of breakthrough time measurements made for idealized channel cases.

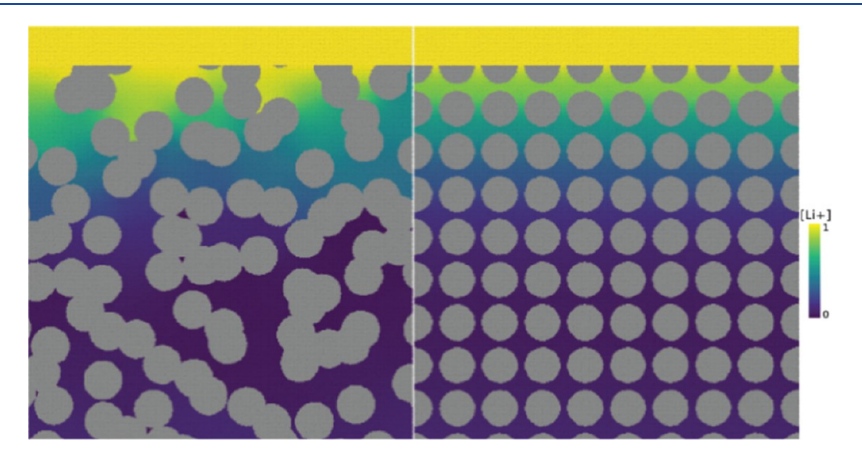


Figure 6. Simulations of diffusion through a porous separator with constant concentration boundary conditions at the top and bottom of the domain for circular inclusions that are randomly placed (left) and regularly placed (right) at the same overall porosity.

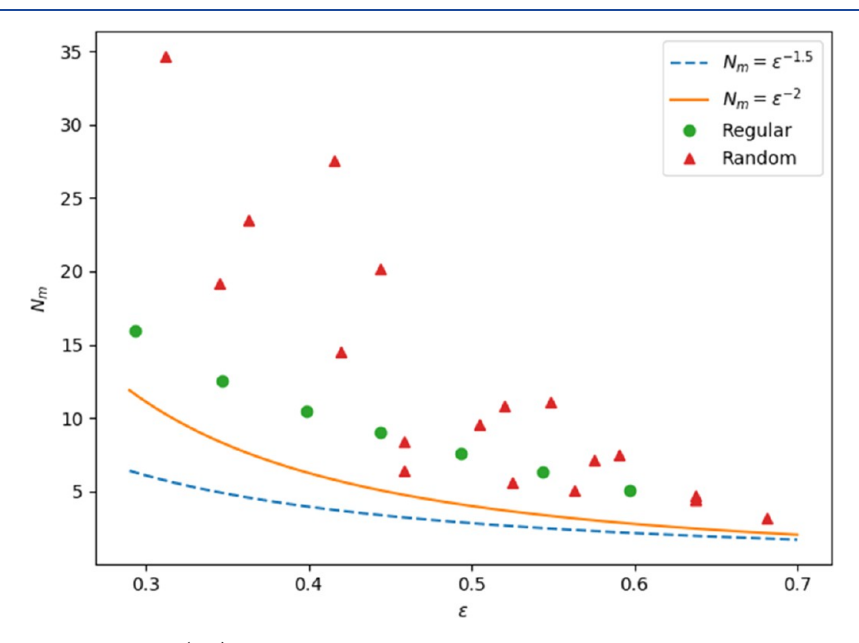


Figure 7. Comparison of MacMullin number $(N_{\rm m})$ to porosity for regularly and randomly placed circular inclusions.

was selected because the main objective is the avoidance of this behavior, i.e., dendrites penetrating and growing through separators. The breakthrough times are normalized against the time it takes for a dendrite to grow to the breakthrough line without a separator in the electrolyte of the simulation.

In the parametric studies discussed in this paper, the molecular diffusivity of the electrolyte and the reaction rate of precipitation are held constant. This allows our discussion to focus on the effects of altering the geometric parameters on dendrite growth. The breakthrough time provides a quantitative measurement for these studies. While this may not be the perfect metric, there are no other metrics to correlate the heterogeneities of a separator and the subsequent dendrite growth. The authors have found no experimental data that tries to relate

these phenomena, most likely because doing so is extremely difficult with current techniques. However, as stated previously, nonuniform mass transport to and at the anode surface is the main driver in dendrite growth. The breakthrough time metric is one way to evaluate this relationship.

4. RESULTS AND DISCUSSION

Four different scenarios were considered to understand the effects of separator microstructure on mass transport and dendrite growth. The first two scenarios explore the relationship between the mass transport and microstructure (excluding

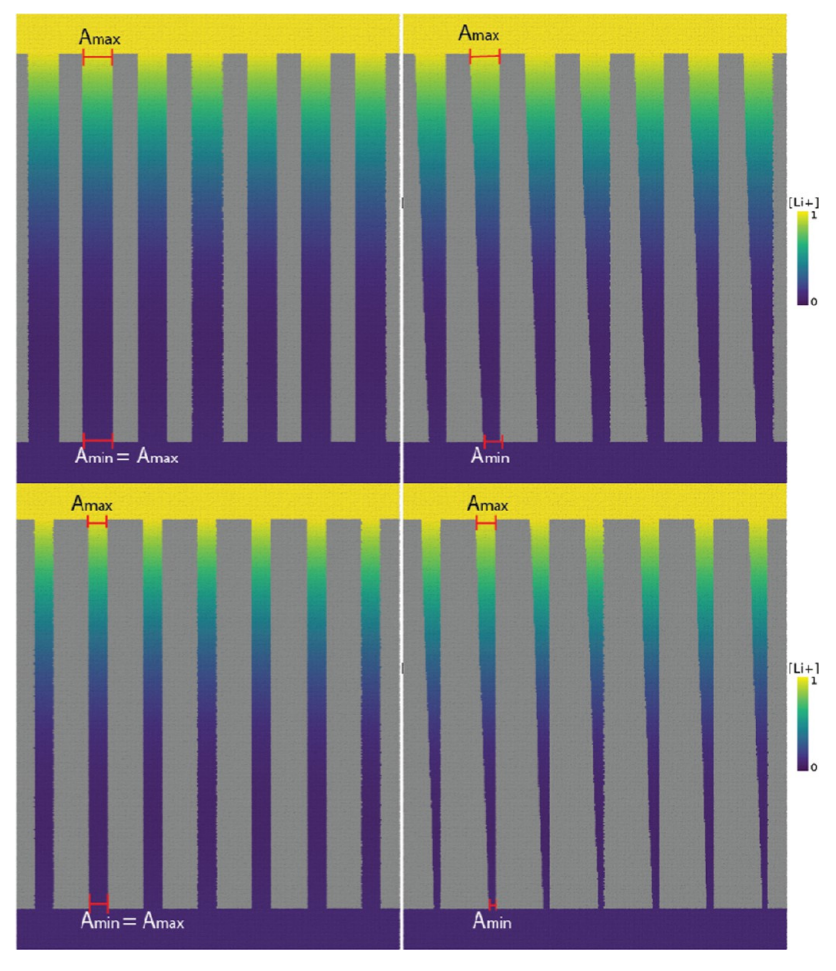


Figure 8. Idealized separator channels for altering constrictivity. Top row (case B) has a lower porosity than the bottom row (case C). Left side has no constrictivity; β is unity.

dendrite growth). The last two scenarios include dendrite growth.

First, both regularly and randomly created, porous geometries are studied to determine how the theoretical relations of Bruggeman and MacMullin compare to the explicitly measured microstructure. Second, due to the difficulty in decoupling constrictivity, porosity, and tortuosity in porous separators, idealized homogeneous channel separators are created to highlight the effect these parameters have on the MacMullin number (eq 1). In the third scenario, two idealized heterogeneous channel separators are compared to understand both the MacMullin number and dendrite growth using the breakthrough time. The last scenario explicitly models the microstructure of Celgard separators to explore the effect its complicated, heterogeneous microstructure has on the MacMullin number and dendrite growth.

4.1. Circular Inclusions and Bruggeman and MacMullin Correlations. The first scenario examines the accuracy of the relations laid out by Bruggeman, which relates the MacMullin number to the porosity (eq 6). For this scenario, simulation domains with both regularly spaced and randomly spaced circular inclusions are used (Figure 6). (The center position of the inclusions is selected using the random number generator in the numpy package in Python. The porosity was varied by changing the radius of the circular inclusions. As can be seen in Figure 6, for a given porosity, a uniform radius was used for all inclusions.

For each test, the SPH simulation was run to calculate an effective diffusivity for the porous separator, using the approach described in Section 3.1. This effective diffusivity was then used to calculate the MacMullin number via eqs 1 and 12.

In Figure 7, a comparison is made between the MacMullin number calculated with the SPH model (eq 1) and the MacMullin number predicted using eq 4 with the porosity varied and the two common α values used in eq 4. For regularly spaced inclusions, the MacMullin number predicted by eq 4 is lower than that predicted by the SPH model by approximately four across all porosities. For randomly spaced inclusions, there is little predictive ability from eq 4 even if the general trend (that the MacMullin number decreases with increasing porosity) is correct. The results of Figure 7 show that the empirical relation of eq 4 is not able to accurately predict the MacMullin number.

4.2. Idealized, Homogeneous Geometries and Bruggeman and MacMullin Correlations. Idealized channel separators are utilized to simplify and understand the effects of the porosity, tortuosity, and constrictivity on mass transport. The idealized channel separators allow different separator characteristics to be decoupled. The constrictivity is isolated first, then the porosity and tortuosity. This scenario tests the assumptions made in eqs 3b and 4 and is frequently used when characterizing separators. Using the approach laid out in Section 3.2, the SPH model is used to calculate the effective diffusivity and MacMullin number, as discussed in Section 3.1.

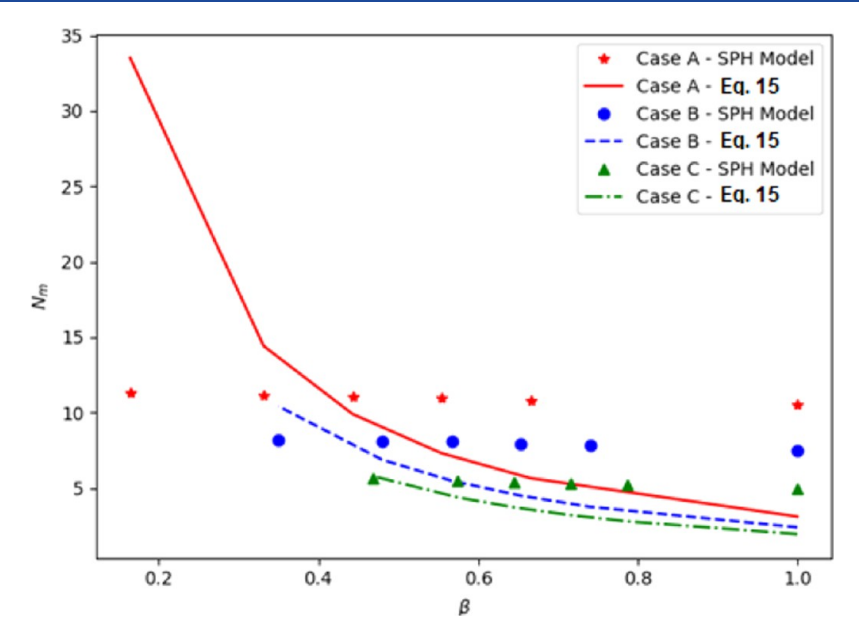


Figure 9. Comparison of MacMullin number (N_m) calculated from the pore-scale SPH model to that predicted by eq 13.

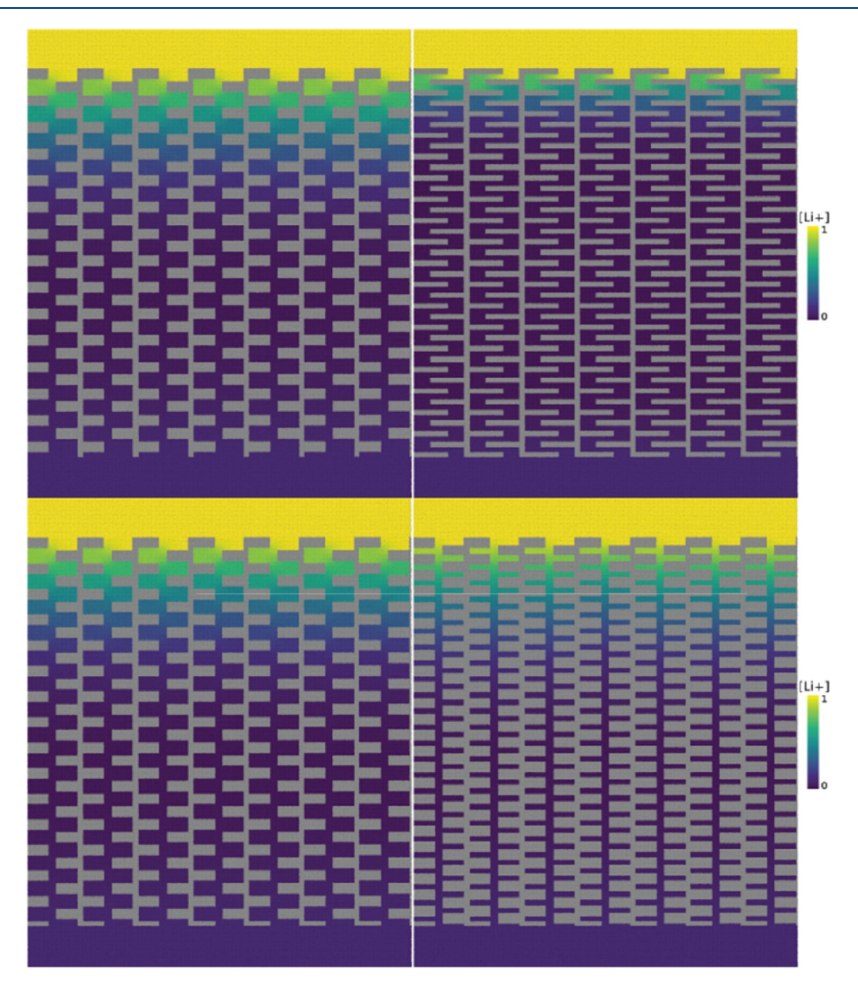


Figure 10. Idealized channel separators used to decouple porosity and tortuosity for $N_{\rm m}$ calculations. Top-row images are simulations with the same porosity and different tortuosities and bottom row images are simulations with different porosities and the same tortuosities.

To understand how constrictivity (β) impacts the effective diffusivity and the MacMullin number, three cases (A, B, C) of channel geometries were considered. The cases start with a constrictivity of 1 (straight, even channels) at three different

porosities: 0.605 for A, 0.494 for B, and 0.384 for C. Then, the channels are increasingly constricted, which decreases the β value and the porosity. All cases have a tortuosity of 1.2. The constrictivity of each case is calculated via eq 2, where A_{\min} and

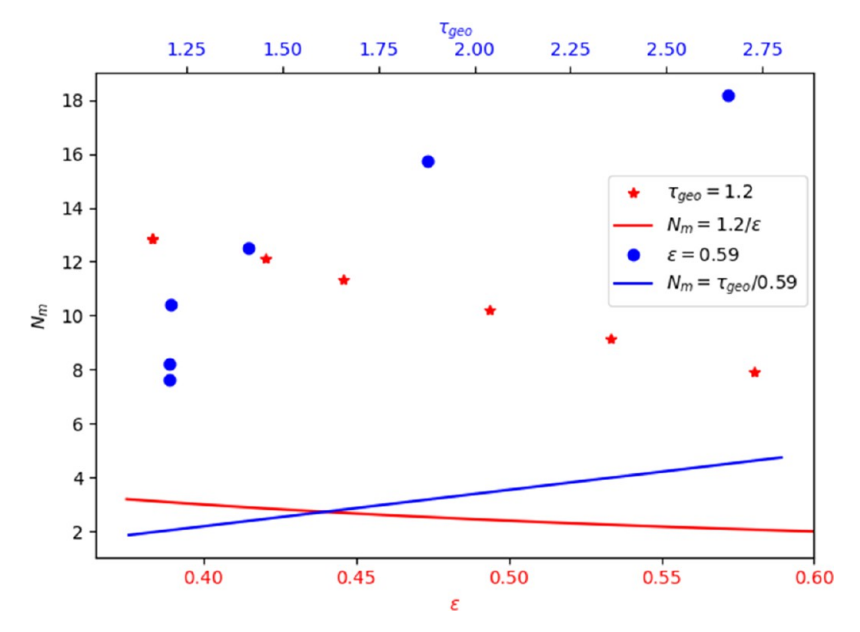


Figure 11. Data from two sets of idealized channel separator simulations and their corresponding empirical $N_{\rm m}$ predictions (solid lines) of eq 4. The red star is the simulation data for varying porosities with a constant tortuosity of 1.2. The blue circle is the simulation data for varying tortuosities with a constant porosity of 0.59.

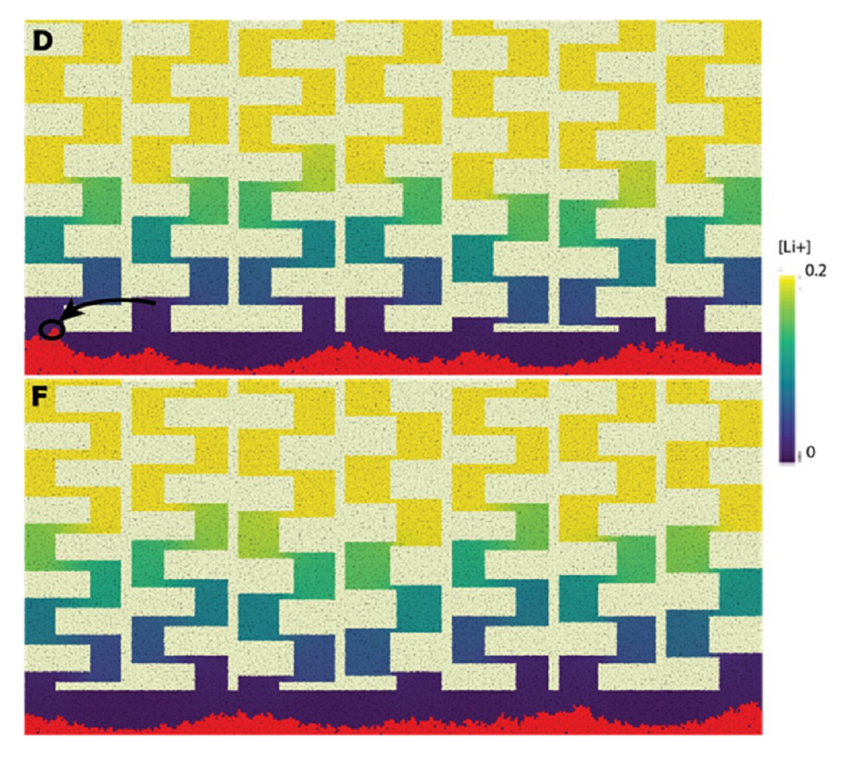


Figure 12. Idealized heterogeneous channel separators with dendrite growth along the anode (bottom, red). The geometry inside each channel is varied producing heterogeneity of both porosity and tortuosity throughout the domain. The average values of porosity and tortuosity are the same, but the range is different resulting in different breakthrough times. All images were taken at the same time.

 $A_{\rm max}$ are defined as shown in Figure 8. Decreasing the constrictivity has an impact on porosity. However, the purpose of these cases is to isolate the constrictivity and determine if it impacts the MacMullin number beyond its impact on the porosity.

The MacMullin number calculated by the effective diffusivity of the pore-scale SPH model is compared to the empirical relations rewritten in terms of $\tau_{\rm geo}$, which accounts for constrictivity, by combining eqs 3b and 4

$$N_{\rm m} = \frac{\tau_{\rm geo}}{\varepsilon} \tag{13}$$

Note that eq 13 simplifies to eq 4 when β goes to unity.

As seen in Figure 9, the MacMullin number calculated via eq 13 has a large dependence on the constrictivity, while the SPH model shows the MacMullin number to be nearly independent of constrictivity (β). Additionally, when constrictivity goes to unity, eq 13 is equal to eq 4, even in this case, the relationship

Table 1. Microstructural Properties and Calculated MacMullin Numbers for Idealized Heterogeneous Channel Separators

	porosity $(arepsilon)$			tortuosity $(au_{ m geo})$			N_{m} calculated from the SPH model			breakthrough time		
	average	min	max	average	min	max	average	min	max	average	min	max
Case D	0.45	0.43	0.48	1.63	1.40	1.96	14.70	13.01	17.21	8.03	6.85	8.83
Case E	0.55	0.53	0.58	1.24	1.21	1.35	8.54	6.81	10.72	3.76	2.65	5.35
Case F	0.45	0.43	0.48	1.63	1.53	1.82	14.90	13.76	16.02	7.79	7.11	8.71
Case G	0.55	0.53	0.59	1.22	1.19	1.25	8.92	7.42	9.96	3.59	3.17	4.06

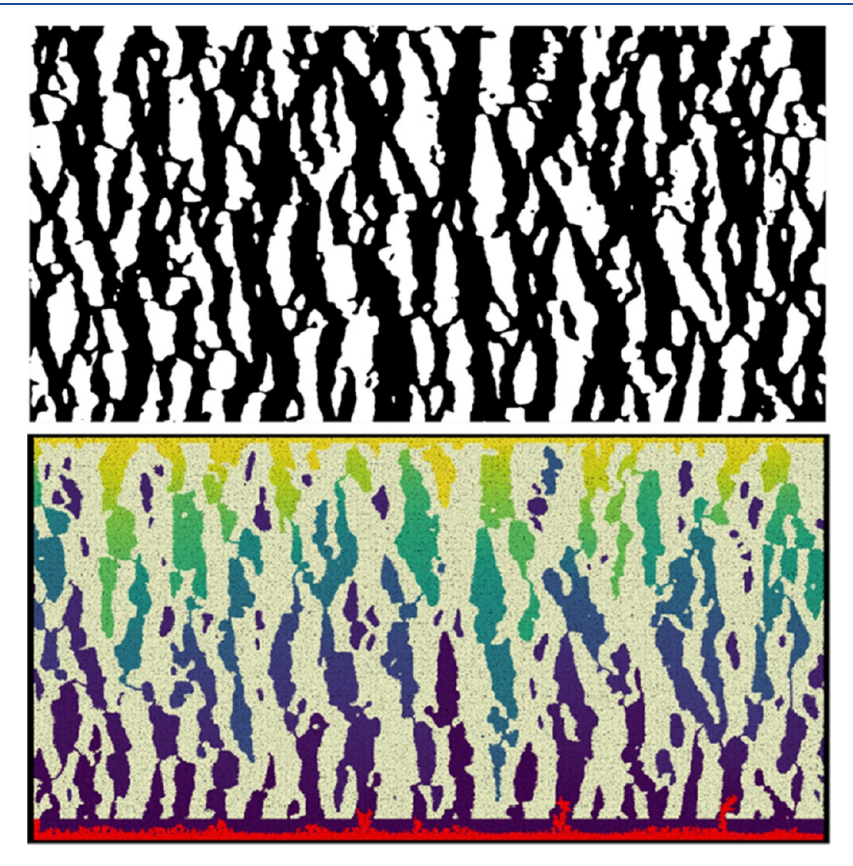


Figure 13. (Top) SEM image of the Celgard separator with the white region as pores and the black region as a separator ("Microstructure of Celgard PP1615 Lithium-Ion Battery Separator" by M. Lagadec et al. is licensed under CC BY-NC-SA 4.0). ⁵³ (Bottom) Image of simulation of diffusion and dendrite growth using the Celgard separator with the colored region as an electrolyte and the off-white region as a separator.

predicts a different MacMullin number then that calculated from the actual effective diffusivity (from the SPH model).

To further explore the effects of geometric parameters on predictions of the MacMullin number, porosity and tortuosity were considered using baffled channels, which allow decoupling between porosity and tortuosity (Figure 10).

Two testing campaigns were conducted: the first has a constant tortuosity and varying porosity and the second has a constant porosity and varying tortuosity. The simulation results in Figure 11 show that the MacMullin number decreases nearly linearly (red symbol) with increasing porosity (and constant tortuosity). Alternatively, as tortuosity increases (blue symbol) MacMullin number increases (with constant porosity).

The values of the MacMullin numbers calculated from the correlation of eq 4 with the measured porosity and tortuosity of the channel structures are presented in Figure 11 as solid lines. The correlation of eq 4 varies significantly from the numerical results (symbols), which calculate the actual effective diffusivity of the channel structure. It suggests that tortuosity is an important property to consider for determining the impact a battery separator has on mass transport and that direct

measurements of tortuosity should be made. Using an experimental fit with porosity values is not sufficient to capture the effects of microstructure.

4.3. Idealized Heterogeneous Microstructures. The scenarios considered in the previous subsections show that the geometric properties of the separator have a significant effect on predicted MacMullin numbers and that many of the empirical relations (eqs 4,6, and 13) do not capture the full effects of the porosity, tortuosity, and constrictivity on effective diffusivity and MacMullin number. In addition to the geometric parameters, the heterogeneity of the separator also plays a critical role in the overall and local mass transport through the separator. Often the bulk measurements of different separators can be similar, but this does not necessarily mean that the distributions of these characteristics are similar. The bulk measurements can obscure imperfections in the separators, which lead to problematic dendritic growth.

To study the effect of heterogeneity, simulations with the idealized baffled channel geometry but differing tortuosity and porosity for each channel were used (Figure 12). In the contour plots of Figure 12, the Li plating (red) is occurring nonuniformly

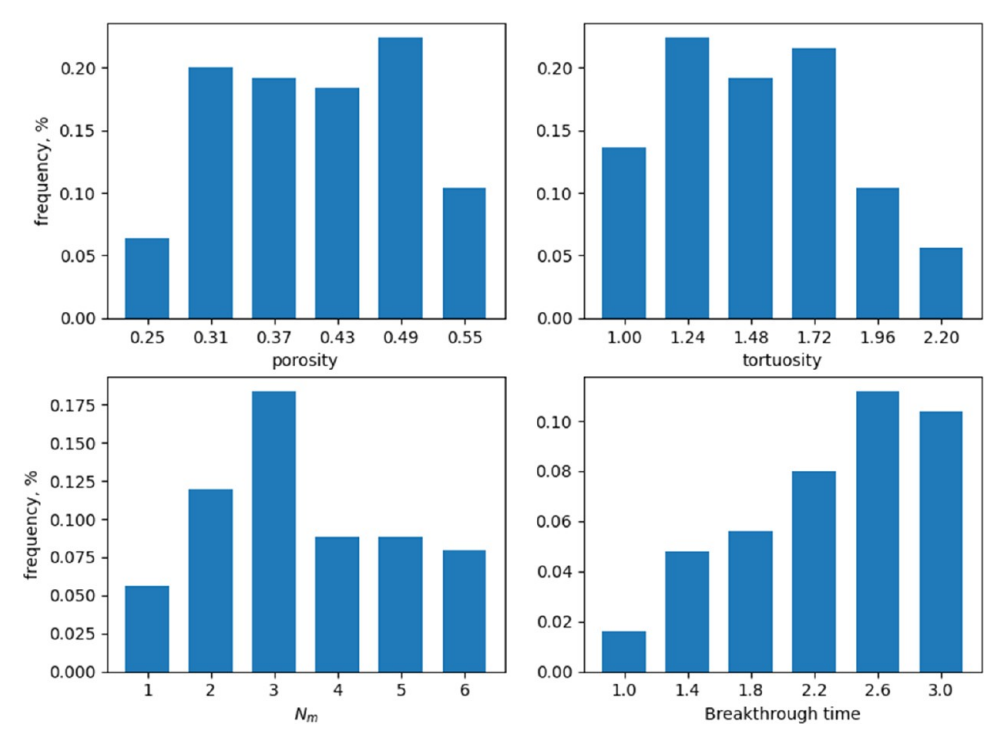


Figure 14. Histograms of microstructural properties and effects on diffusivity and dendrite growth. Porosity and tortuosity (top row) measurements are made along 0.5 μ m sections of the separator. The MacMullin number and breakthrough time are calculated for the same sections (bottom row).

across the bottom of the domain. The uneven plating leads to run away dendrite growth, which can lead to safety issues. As indicated in Table 1, four cases were considered (D, E, F, G) which each have a range of porosities and tortuosities throughout their domains.

For these simulations, the MacMullin number is calculated as discussed in the previous subsections, and dendritic growth is also included. Dendrite growth is included via a reactive boundary condition at the bottom of the simulation domain (eq 10).

The local MacMullin number is calculated for individual channels within the domain. As shown in Table 1, Cases D and F have similar average geometrical properties, and Cases E and G have similar average geometrical properties. For both sets of cases (D and F, and E and G), there is a large range of local MacMullin numbers but similar averages. There are two sets of cases so the degree of heterogeneity can be examined. Cases D and E have larger ranges of tortuosities, while cases F and G have smaller ranges of tortuosities. Tortuosity was altered in this manner because in the previous section it was found to contribute more significantly to the MacMullin number than the porosity.

These cases were selected so that their average MacMullin numbers and the average geometric properties would be similar. They further show that even if the averages are similar, inside the separator, the properties can vary dramatically. A breakthrough occurs 5% sooner in case D despite case D having similar bulk diffusivity to case F (Figure 12). A breakthrough occurs 15% sooner in case E despite case E having similar bulk diffusivity to case G. Therefore, measuring the bulk effective diffusivity will not provide any information about the heterogeneity of a separator's microstructure. This is critical in battery separators because dendrite growth is known to nucleate near heterogeneities and the growth rate will depend on local mass transport, not an effective bulk transport.

4.4. Heterogeneity and Dendrite Growth with Celgard Separators. Although the previous idealized cases offered some insight into the effects of heterogeneous microstructure on mass transport and dendrite growth, further insight can be achieved using explicit representations of Celgard separators. These separators were imaged with a SEM at 10 nm resolution (Figure 13 top) by Woods et al.⁷³ The microstructure was reconstructed from these SEM images for use in the SPH modeling of this work. In the simulation, the resolution is upscaled to 20 nm per model particle (Figure 13 bottom).

The dimensions of the separator slice are $13~\mu m \times 6.5~\mu m$ and five slices were used in different simulations. To translate the separator into 2-D, small edits were made to ensure open pores. To measure the heterogeneity of the separator's microstructure, each separator was divided into 26 regions, measuring $0.5~\mu m \times 6.5~\mu m$. The region shapes were selected to roughly capture the pathways that Li ions travel during charging. They are also at the scale of initial dendritic growth. The porosity, tortuosity, effective diffusivity, and breakthrough time were calculated from the SPH simulations for each region. The ranges of these measurements are shown in Figure 14.

The bulk porosity, tortuosity, and MacMullin number for the Celgard separator reported by Wood et al. ⁷⁴ are, respectively, 0.402, 2.31, and 5.68 and are similar to the bulk values in this work. The range of porosity and tortuosity values lead to a range of MacMullin numbers and breakthrough times. However, the bulk values are only reported by the manufacturer and do not capture some regions that have lower MacMullin numbers (faster transport). Regions have lower MacMullin numbers because the local microstructure, e.g., porosity and tortuosity, does not restrict transport as severely as regions with higher MacMullin numbers. In Figure 15, a region of the separator is highlighted to show the higher porosity (0.49) and lower tortuosity (1.1), which leads to a lower MacMullin number (1.6).

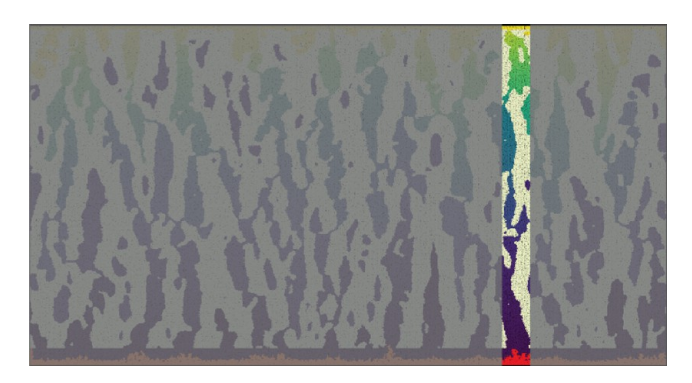


Figure 15. Region of the Celgard separator with higher porosity, lower tortuosity, and lower MacMullin number. This region has a lower breakthrough time compared to the rest of this separator. This region exhibits faster dendrite growth that would not be evident if the separator was only characterized by its bulk characteristics.

The regions with lower MacMullin numbers are the regions that have the shortest breakthrough time. This indicates that these regions have dendrites that grow much faster than others which can lead to battery failure. The results of the simulations using the Celgard separators and dendrite growth suggest that using highly homogenous battery separators could suppress dendrite growth. A homogeneous battery separator would create uniform mass transport through the electrolyte and uniform deposition on the anode surface.

5. CONCLUSIONS

The current empirical methods for calculating the tortuosity, MacMullin number, and effective diffusivity do not capture the full effects that the microstructure has on these parameters and are inadequate for determining the effect a battery's separator will have on dendritic growth. Describing the MacMullin number as a simple function of porosity (eq 6) neglects the effects of tortuosity on local mass transfer, which we show has a significant effect on the effective diffusivity and MacMullin number. Additionally, calculating the tortuosity from empirical relations that are only a function of porosity ignores that microstructures can have the same porosity but different tortuosities as shown in Figure 11 and Section 4.4. It has been demonstrated that these parameters need to be measured independently. In addition, the influence of constrictivity on MacMullin number is significantly less than that predicted by empirical relations (eq 13). Care should be taken in the use of empirical relations, with the understanding that their accuracy is not guaranteed and that they were developed based on a fit to a specific data set and are not universally applicable.

In addition to the measurement and calculation of microstructural parameters, there is also the challenge of accounting for heterogeneities in the microstructure. Bulk parameters, such as porosity and tortuosity, can be misleading when determining the cause of failure in a battery and are not sufficient when developing complex and potentially dangerous technologies such as Li batteries. As Sections 4.3 and 4.4 discuss, microstructures with the same average (bulk) properties predict significantly different breakthrough times for dendrite growth due to the strong influence of local properties and mass transport on dendrite growth. The heterogeneous microstructure of battery separators should be considered in the design of new systems and in the study of battery failure. This is clearly seen in the experimental Celgard separator, which is considered in Section 4.4. The model is able to accurately predict the

experimental MacMullin number; however, local heterogeneities that are not captured by the MacMullin number are critical to dendrite growth.

More control over and understanding of ranges of values of local properties are needed, and the ability to manufacture more homogeneous battery separators are needed to ensure more uniform mass transport inside the electrolyte and suppression of dendritic growth. Increased control over the separator microstructure through advanced fabrication techniques could improve battery performance and become an important area of experimental design for advanced batteries. Finally, better characterization tools that can resolve the separator microstructures and their effects on local ion concentrations and operando changes in the electrode interface could improve modeling efforts and lead to more powerful integrated computational—experimental design paradigms.

AUTHOR INFORMATION

Corresponding Author

Emily M. Ryan — Department of Mechanical Engineering, Boston University, Boston, Massachusetts 02215, United States; orcid.org/0000-0001-6111-3269; Email: ryanem@bu.edu

Author

Andrew Cannon — Department of Mechanical Engineering, Boston University, Boston, Massachusetts 02215, United States; orcid.org/0000-0002-8750-6199

Complete contact information is available at: https://pubs.acs.org/10.1021/acsaem.1c00144

Notes

The authors declare no competing financial interest.

ACKNOWLEDGMENTS

Partial financial support for this research is provided by the National Science Foundation through award numbers 1911698 and 2034154. The authors would like to acknowledge Quang-Thinh Ha for his helpful discussions and assistance in implementing Tartakovsky et al.'s algorithm⁶⁷ for reactive transport and precipitation into LAMMPS.

REFERENCES

- (1) Babiker, M.; Bertoldi, P.; Buckeridge, M.; Cartwright, A.; Araos Maldives, M.; Bakker, S.; Bazaz, A.; Belfer, E.; Benton, T.; de Coninck, H.; Revi, A.; Babiker, M.; Bertoldi, P.; Buckeridge, M.; Cartwright, A.; Dong, W.; Ford, J.; Fuss, S.; Hourcade, J.; Ley, D.; Mechler, R.; Newman, P.; Revokatova, A.; Schultz, S.; Steg, L.; Sugiyama, T.; Masson-Delmotte, V.; Zhai, P.; Pörtner, H. O.; Roberts, D.; Skea, J.; Shukla, P.; Pirani, A.; Moufouma-Okia, W.; Péan, C.; Pidcock, R.; Connors, S.; R Matthews, J. B.; Chen, Y.; Zhou, X.; Gomis, M. I.; Lonnoy, E.; Maycock, T.; Tignor, M.; Waterfield, T. Strengthening and Implementing the Global Response. In *Global Warming of 1.5 °C*, **2018**; Chapter 4.
- (2) Aifantis, K. E.; Hackney, S. A.; Kumar, R. V. High Energy Density Lithium Batteries: Materials, Engineering, Applications; 2010.
- (3) Cheng, X. B.; Zhang, R.; Zhao, C. Z.; Zhang, Q. Toward Safe Lithium Metal Anode in Rechargeable Batteries: A Review. *Chem. Rev.* **2017**, *117*, 10403–10473.
- (4) Brissot, C.; Rosso, M.; Chazalviel, J. N.; Lascaud, S. Dendritic Growth Mechanisms in Lithium/Polymer Cells. *J. Power Sources* **1999**, 81–82, 925–929.
- (5) Monroe, C.; Newman, J. Dendrite Growth in Lithium/Polymer Systems. J. Electrochem. Soc. 2003, 150, No. A1377.

- (6) Cheng, X.-B.; Zhang, R.; Zhao, C. Z.; Zhang, Q. Toward Safe Lithium Metal Anode in Rechargeable Batteries: A Review. *Chem. Rev.* **2017**, *117*, 10403–10473.
- (7) Becking, J.; Gröbmeyer, A.; Kolek, M.; Rodehorst, U.; Schulze, S.; Winter, M.; Bieker, P.; Stan, M. C. Lithium-Metal Foil Surface Modification: An Effective Method to Improve the Cycling Performance of Lithium-Metal Batteries. *Adv. Mater. Interfaces* **2017**, 4, No. 1700166.
- (8) Jana, A.; García, R. E. Lithium Dendrite Growth Mechanisms in Liquid Electrolytes. *Nano Energy* **2017**, *41*, 552–565.
- (9) Wood, K. N.; Kazyak, E.; Chadwick, A. F.; Chen, K. H.; Zhang, J. G.; Thornton, K.; Dasgupta, N. P. Dendrites and Pits: Untangling the Complex Behavior of Lithium Metal Anodes through Operando Video Microscopy. ACS Cent. Sci. 2016, 2, 790–801.
- (10) Chazalviel, J.-N. Electrochemical Aspects of the Generation of Ramified Metallic Electrodeposits. *Phys. Rev. A* **1990**, *42*, 7355–7367. (11) Tan, J.; Ryan, E. M. Numerical Modeling of Dendrite Growth in a
- Lithium Air Battery System. ECS Trans. 2013, 53, 35–43.
- (12) Hao, Z.; Zhao, Q.; Tang, J.; Zhang, Q.; Liu, J.; Jin, Y.; Wang, H. Functional Separators towards the Suppression of Lithium Dendrites for Rechargeable High-Energy Batteries. *Mater. Horizons* **2021**, *8*, 12–32.
- (13) Yang, Y.; Wang, W.; Li, L.; Li, B.; Zhang, J. Stable Cycling of Li-S Batteries by Simultaneously Suppressing Li-Dendrite Growth and Polysulfide Shuttling Enabled by a Bioinspired Separator. *J. Mater. Chem. A* **2020**, *8*, 3692–3700.
- (14) Nie, L.; Li, Y.; Chen, S.; Li, K.; Huang, Y.; Zhu, Y.; Sun, Z.; Zhang, J.; He, Y.; Cui, M.; Wei, S.; Qiu, F.; Zhong, C.; Liu, W. Biofilm Nanofiber-Coated Separators for Dendrite-Free Lithium Metal Anode and Ultrahigh-Rate Lithium Batteries. *ACS Appl. Mater. Interfaces* **2019**, *11*, 32373–32380.
- (15) Wang, J.; Yi, S.; Liu, J.; Sun, S.; Liu, Y.; Yang, D.; Xi, K.; Gao, G.; Abdelkader, A.; Yan, W.; Ding, S.; Kumar, R. V. Suppressing the Shuttle Effect and Dendrite Growth in Lithium-Sulfur Batteries. *ACS Nano* **2020**, *14*, 9819–9831.
- (16) Rajendran, S.; Tang, Z.; George, A.; Cannon, A.; Neumann, C.; Sawas, A.; Ryan, E.; Turchanin, A.; Arava, L. M. R. Inhibition of Lithium Dendrite Formation in Lithium Metal Batteries via Regulated Cation Transport through Ultrathin Sub-Nanometer Porous Carbon Nanomembranes. *Adv. Energy Mater.* **2021**, No. 2100666.
- (17) Zhang, X.; Wang, Q. J.; Harrison, K. L.; Jungjohann, K.; Boyce, B. L.; Roberts, S. A.; Attia, P. M.; Harris, S. J. Rethinking How External Pressure Can Suppress Dendrites in Lithium Metal Batteries. *J. Electrochem. Soc.* **2019**, *166*, A3639—A3652.
- (18) Liang, J.; Chen, Q.; Liao, X.; Yao, P.; Zhu, B.; Lv, G.; Wang, X.; Chen, X.; Zhu, J. A Nano-Shield Design for Separators to Resist Dendrite Formation in Lithium-Metal. *Angew. Chem. Int. Ed.* **2020**, 59, 6561–6566.
- (19) Lee, H.; Ren, X.; Niu, C.; Yu, L.; Engelhard, M. H.; Cho, I.; Ryou, M. H.; Jin, H. S.; Kim, H. T.; Liu, J.; Xu, W.; Zhang, J. G. Suppressing Lithium Dendrite Growth by Metallic Coating on a Separator. *Adv. Funct. Mater.* **2017**, *27*, No. 1704391.
- (20) Nagasaki, M.; Kanamura, K. High-Performance Lithium Metal Rechargeable Battery Using an Ultrafine Porous Polyimide Separator with Three-Dimensionally Ordered Macroporous Structure. *ACS Appl. Energy Mater.* **2019**, *2*, 3896–3903.
- (21) Ma, L.; Chen, R.; Hu, Y.; Zhang, W.; Zhu, G.; Zhao, P.; Chen, T.; Wang, C.; Yan, W.; Wang, Y.; Wang, L.; Tie, Z.; Liu, J.; Jin, Z. Nanoporous and Lyophilic Battery Separator from Regenerated Eggshell Membrane with Effective Suppression of Dendritic Lithium Growth. *Energy Storage Mater.* **2018**, *14*, 258–266.
- (22) Rao, Z.; Meng, J.; Wu, J.; Yu, S.; Fu, Q.; Huang, Y. A Multifunctional Inorganic Composite Separator for Stable High-Safety Lithium-Sulfur Batteries. *ACS Appl. Energy Mater.* **2020**, *3*, 10139–10146.
- (23) Holzer, L.; Wiedenmann, D.; Münch, B.; Keller, L.; Prestat, M.; Gasser, P.; Robertson, I.; Grobéty, B. The Influence of Constrictivity on the Effective Transport Properties of Porous Layers in Electrolysis and Fuel Cells. *J. Mater. Sci.* **2013**, *48*, 2934–2952.

- (24) García-García, R.; García, R. E. Microstructural Effects on the Average Properties in Porous Battery Electrodes. *J. Power Sources* **2016**, 309, 11–19.
- (25) Tjaden, B.; Cooper, S. J.; Brett, D. J.; Kramer, D.; Shearing, P. R. On the Origin and Application of the Bruggeman Correlation for Analysing Transport Phenomena in Electrochemical Systems. *Curr. Opin. Chem. Eng.* **2016**, *12*, 44–51.
- (26) Chung, D.-W.; Ebner, M.; Ely, D. R.; Wood, V.; Edwin García, R. Validity of the Bruggeman Relation for Porous Electrodes. *Model. Simul. Mater. Sci. Eng.* **2013**, *21*, No. 074009.
- (27) Tjaden, B.; Brett, D. J. L.; Shearing, P. R. Tortuosity in Electrochemical Devices: A Review of Calculation Approaches. *Int. Mater. Rev.* **2016**, *63*, 47–67.
- (28) Zacharias, N. A.; Nevers, D. R.; Skelton, C.; Knackstedt, K.; Stephenson, D. E.; Wheeler, D. R. Direct Measurements of Effective Ionic Transport in Porous Li-Ion Electrodes. *J. Electrochem. Soc.* **2013**, *160*, A306–A311.
- (29) Usseglio-Viretta, F. L. E.; Colclasure, A.; Mistry, A. N.; Claver, K. P. Y.; Pouraghajan, F.; Finegan, D. P.; Heenan, T. M. M.; Abraham, D.; Mukherjee, P. P.; Wheeler, D.; Shearing, P.; Cooper, S. J.; Smith, K. Resolving the Discrepancy in Tortuosity Factor Estimation for Li-Ion Battery Electrodes through Micro-Macro Modeling and Experiment. *J. Electrochem. Soc.* **2018**, *165*, A3403—A3426.
- (30) Armatas, G. S. Determination of the Effects of the Pore Size Distribution and Pore Connectivity Distribution on the Pore Tortuosity and Diffusive Transport in Model Porous Networks. *Chem. Eng. Sci.* **2006**, *61*, 4662–4675.
- (31) Salem, H. S.; Chilingarian, G. V. Physical and Mathematical Aspects of Tortuosity in Regard to the Fluid Flow and Electric Current Conduction in Porous Media: Example of the Hibernia and Terra Nova Reservoirs, off the Eastern Coast of Canada. *Energy Sources* **2000**, 22, 137–145.
- (32) Kalnaus, S.; Wang, Y.; Turner, J. A. Mechanical Behavior and Failure Mechanisms of Li-Ion Battery Separators. *J. Power Sources* **2017**, 348, 255–263.
- (33) Lagadec, M. F.; Zahn, R.; Wood, V. Characterization and Performance Evaluation of Lithium-Ion Battery Separators. *Nature Energy* **2019**, *4*, 16–25.
- (34) Kehrwald, D.; Shearing, P. R.; Brandon, N. P.; Sinha, P. K.; Harris, S. J. Local Tortuosity Inhomogeneities in a Lithium Battery Composite Electrode. *J. Electrochem. Soc.* **2011**, *158*, No. A1393.
- (35) Lu, D.; Shao, Y.; Lozano, T.; Bennett, W. D.; Graff, G. L.; Polzin, B.; Zhang, J.; Engelhard, M. H.; Saenz, N. T.; Henderson, W. A.; Bhattacharya, P.; Liu, J.; Xiao, J. Failure Mechanism for Fast-Charged Lithium Metal Batteries with Liquid Electrolytes. *Adv. Energy Mater.* **2015**, *5*, No. 1400993.
- (36) Tan, J.; Ryan, E. M. Structured Electrolytes to Suppress Dendrite Growth in High Energy Density Batteries. *Int. J. Energy Res.* **2016**, *40*, 1800–1810.
- (37) Arora, P.; Zhang, Z. Battery Separators. Chem. Rev. 2004, 104, 4419–4462.
- (38) Kim, J.-K.; Kim, D. H.; Joo, S. H.; Choi, B.; Cha, A.; Kim, K. M.; Kwon, T. H.; Kwak, S. K.; Kang, S. J.; Jin, J. Hierarchical Chitin Fibers with Aligned Nanofibrillar Architectures: A Nonwoven-Mat Separator for Lithium Metal Batteries. *ACS Nano* **2017**, *11*, 6114–6121.
- (39) Korthauer, R. Lithium-Ion Batteries: Basics and Applications; Springer, 2018.
- (40) Newman, J.; Thomas-Alyea, K. E. K. E. Electrochemical Systems; John Wiley & Sons, Inc, 2004.
- (41) Thorat, I. V.; Stephenson, D. E.; Zacharias, N. A.; Zaghib, K.; Harb, J. N.; Wheeler, D. R. Quantifying Tortuosity in Porous Li-Ion Battery Materials. *J. Power Sources* **2009**, *188*, 592–600.
- (42) Landesfeind, J.; Hattendorff, J.; Ehrl, A.; Wall, W. A.; Gasteiger, H. A. Tortuosity Determination of Battery Electrodes and Separators by Impedance Spectroscopy. *J. Electrochem. Soc.* **2016**, *163*, A1373—A1387.
- (43) Epstein, N. On Tortuosity and the Tortuosity Factor in Flow and Diffusion through Porous Media. *Chem. Eng. Sci.* **1989**, 44, 777–779.

- (44) MacMullin, R. B.; Muccini, G. A. Characteristics of Porous Beds and Structures. *AIChE J.* **1956**, 2, 393–403.
- (45) Zhang, S. S. A Review on the Separators of Liquid Electrolyte Li-Ion Batteries. *J. Power Sources* **2007**, *164*, 351–364.
- (46) Ullman, W. J.; Aller, R. C. Diffusion Coefficients in Nearshore Marine Sediments 1. *Limnol. Oceanogr.* **1982**, *27*, 552–556.
- (47) Wiedenmann, D.; Keller, L.; Holzer, L.; Stojadinović, J.; Münch, B.; Suarez, L.; Fumey, B.; Hagendorfer, H.; Brönnimann, R.; Modregger, P.; Gorbar, M.; Vogt, U. F.; Züttel, A.; Mantia, F. La.; Wepf, R.; Grobéty, B. Three-Dimensional Pore Structure and Ion Conductivity of Porous Ceramic Diaphragms. *AIChE J.* **2013**, *59*, 1446–1457.
- (48) Engblom, S. O.; Myland, J. C.; Oldham, K. B.; Taylor, A. L.; Topic, W. C. Electrochemical Detection of Large Channels in Porous Rocks. *J. Appl. Electrochem.* **2003**, 33, 51–59.
- (49) Bruggeman, D. A. G. Berechnung Verschiedener Physikalischer Konstanten von Heterogenen Substanzen. I. Dielektrizitätskonstanten Und Leitfähigkeiten Der Mischkörper Aus Isotropen Substanzen. *Ann. Phys.* **1935**, *416*, 636–664.
- (50) Patel, K. K.; Paulsen, J. M.; Desilvestro, J. Numerical Simulation of Porous Networks in Relation to Battery Electrodes and Separators. *J. Power Sources* **2003**, *122*, 144–152.
- (51) Sun, Z.; Tang, X.; Cheng, G. Numerical Simulation for Tortuosity of Porous Media. *Microporous Mesoporous Mater.* **2013**, 173, 37–42.
- (52) Ehrl, A.; Landesfeind, J.; Wall, W. A.; Gasteiger, H. A. Determination of Transport Parameters in Liquid Binary Lithium Ion Battery Electrolytes I. Diffusion Coefficient. *J. Electrochem. Soc.* **2017**, DOI: 10.1149/2.1131704jes.
- (53) Lagadec, M. F. Microstructure of Celgard PP1615 Lithium-Ion Battery Separator. *ETH Zurich.* **2018**, DOI: 10.3929/ethz-b-000265085.
- (54) Steiger, J.; Kramer, D.; Mönig, R. Microscopic Observations of the Formation, Growth and Shrinkage of Lithium Moss during Electrodeposition and Dissolution. *Electrochim. Acta* **2014**, *136*, 529–536.
- (55) Tan, J.; Ryan, E. M. Computational Study of Electro-Convection Effects on Dendrite Growth in Batteries. *J. Power Sources* **2016**, 323, 67–77.
- (56) Tan, J.; Tartakovsky, A. M.; Ferris, K.; Ryan, E. M. Investigating the Effects of Anisotropic Mass Transport on Dendrite Growth in High Energy Density Lithium Batteries. *J. Electrochem. Soc.* **2016**, *163*, A318—A327.
- (57) Zugmann, S.; Fleischmann, M.; Amereller, M.; Gschwind, R. M.; Wiemhöfer, H. D.; Gores, H. J. Measurement of Transference Numbers for Lithium Ion Electrolytes via Four Different Methods, a Comparative Study. *Electrochim. Acta* **2011**, *56*, 3926–3933.
- (58) Elezgaray, J.; Léger, C.; Argoul, F. Linear Stability Analysis of Unsteady Galvanostatic Electrodeposition in the Two-Dimensional Diffusion-Limited Regime. *J. Electrochem. Soc.* **1998**, *145*, 2016–2024.
- (59) Jana, A.; Ely, D. R.; García, R. E. Dendrite-Separator Interactions in Lithium-Based Batteries. *J. Power Sources* **2015**, 275, 912–921.
- (60) Liang, L.; Qi, Y.; Xue, F.; Bhattacharya, S.; Harris, S. J.; Chen, L. Q. Nonlinear Phase-Field Model for Electrode-Electrolyte Interface Evolution. *Phys. Rev. E* **2012**, *86*, No. 051609.
- (61) Yurkiv, V.; Foroozan, T.; Ramasubramanian, A.; Shahbazian-Yassar, R.; Mashayek, F. Phase-Field Modeling of Solid Electrolyte Interface (SEI) Influence on Li Dendritic Behavior. *Electrochim. Acta* **2018**, 265, 609–619.
- (62) Chen, L.; Zhang, H. W.; Liang, L. Y.; Liu, Z.; Qi, Y.; Lu, P.; Chen, J.; Chen, L. Q. Modulation of Dendritic Patterns during Electrodeposition: A Nonlinear Phase-Field Model. *J. Power Sources* **2015**, *300*, 376–385.
- (63) Plimpton, S. Fast Parallel Algorithms for Short-Range Molecular Dynamics. *J. Comput. Phys.* **1995**, *117*, 1–19.
- (64) Leroch, S.; Varga, M.; Eder, S. J.; Vernes, A.; Rodriguez Ripoll, M.; Ganzenmüller, G. Smooth Particle Hydrodynamics Simulation of Damage Induced by a Spherical Indenter Scratching a Viscoplastic Material. *Int. J. Solids Struct.* **2016**, *81*, 188–202.

- (65) Ryan, E.; Pollard, Z. A.; Ha, Q.-T.; Roshandelpoor, A.; Vakili, P.; Goldfarb, J. L. Designing Heterogeneous Hierarchical Material Systems: A Holistic Approach to Structural and Materials Design. *MRS Commun.* **2019**, *9*, 628–636.
- (66) Tan, J.; Cannon, A.; Ryan, E. Simulating Dendrite Growth in Lithium Batteries under Cycling Conditions. *J. Power Sources* **2020**, 463, No. 228187.
- (67) Tartakovsky, A. M.; Meakin, P.; Scheibe, T. D.; Eichler West, R. M. Simulations of Reactive Transport and Precipitation with Smoothed Particle Hydrodynamics. *J. Comput. Phys.* **2007**, 222, 654–672.
- (68) Crank, J. The Mathematics of Diffusion; Oxford University Press, 1979.
- (69) Hart, P. E.; Nilsson, N. J.; Raphael, B. A Formal Basis for the Heuristic Determination of Minimum Cost Paths. *IEEE Trans. Syst. Sci. Cybern.* **1968**, *4*, 100–107.
- (70) Dijkstra, E. W. A Note on Two Problems in Connexion with Graphs. *Numer. Math.* **1959**, *1*, 269–271.
- (71) Virtanen, P.; Gommers, R.; Oliphant, T. E.; Haberland, M.; Reddy, T.; Cournapeau, D.; Burovski, E.; Peterson, P.; Weckesser, W.; Bright, J.; van der Walt, S. J.; Brett, M.; Wilson, J.; Millman, K. J.; Mayorov, N.; Nelson, A. R. J.; Jones, E.; Kern, R.; Larson, E.; Carey, C. J.; Polat, İ.; Feng, Y.; Moore, E. W.; VanderPlas, J.; Laxalde, D.; Perktold, J.; Cimrman, R.; Henriksen, I.; Quintero, E. A.; Harris, C. R.; Archibald, A. M.; Ribeiro, A. H.; Pedregosa, F.; van Mulbregt, P.; Vijaykumar, A.; Bardelli, A.; Pietro; Rothberg, A.; Hilboll, A.; Kloeckner, A.; Scopatz, A.; Lee, A.; Rokem, A.; Woods, C. N.; Fulton, C.; Masson, C.; Häggström, C.; Fitzgerald, C.; Nicholson, D. A.; Hagen, D. R.; Pasechnik, D. V.; Olivetti, E.; Martin, E.; Wieser, E.; Silva, F.; Lenders, F.; Wilhelm, F.; Young, G.; Price, G. A.; Ingold, G. L.; Allen, G. E.; Lee, G. R.; Audren, H.; Probst, I.; Dietrich, J. P.; Silterra, J.; Webber, J. T.; Slavič, J.; Nothman, J.; Buchner, J.; Kulick, J.; Schönberger, J. L.; de Miranda Cardoso, J. V.; Reimer, J.; Harrington, J.; Rodríguez, J. L. C.; Nunez-Iglesias, J.; Kuczynski, J.; Tritz, K.; Thoma, M.; Newville, M.; Kümmerer, M.; Bolingbroke, M.; Tartre, M.; Pak, M.; Smith, N. J.; Nowaczyk, N.; Shebanov, N.; Pavlyk, O.; Brodtkorb, P. A.; Lee, P.; McGibbon, R. T.; Feldbauer, R.; Lewis, S.; Tygier, S.; Sievert, S.; Vigna, S.; Peterson, S.; More, S.; Pudlik, T.; Oshima, T.; Pingel, T. J.; Robitaille, T. P.; Spura, T.; Jones, T. R.; Cera, T.; Leslie, T.; Zito, T.; Krauss, T.; Upadhyay, U.; Halchenko, Y. O.; Vázquez-Baeza, Y. SciPy 1.0: Fundamental Algorithms for Scientific Computing in Python. Nat. Methods 2020, 17, 261-272.
- (72) Harris, C. R.; Millman, K. J.; van der Walt, S. J.; Gommers, R.; Virtanen, P.; Cournapeau, D.; Wieser, E.; Taylor, J.; Berg, S.; Smith, N. J.; Kern, R.; Picus, M.; Hoyer, S.; van Kerkwijk, M. H.; Brett, M.; Haldane, A.; del Río, J. F.; Wiebe, M.; Peterson, P.; Gérard-Marchant, P.; Sheppard, K.; Reddy, T.; Weckesser, W.; Abbasi, H.; Gohlke, C.; Oliphant, T. E. Array Programming with NumPy. *Nature* **2020**, *585*, 357–362.
- (73) Lagadec, M. F.; Ebner, M.; Zahn, R.; Wood, V. Communication—Technique for Visualization and Quantification of Lithium-Ion Battery Separator Microstructure. *J. Electrochem. Soc.* **2016**, *163*, A992—A994.
- (74) Lagadec, M. F.; Zahn, R.; Müller, S.; Wood, V. Topological and Network Analysis of Lithium Ion Battery Components: The Importance of Pore Space Connectivity for Cell Operation. *Energy Environ. Sci.* **2018**, *11*, 3194–3200.